

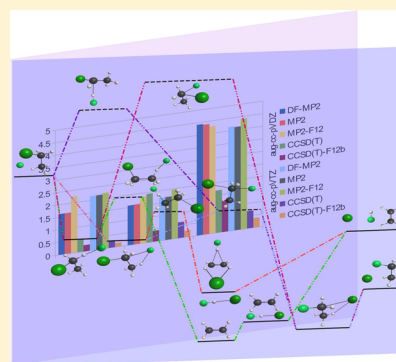
Benchmark ab Initio Characterization of the Complex Potential Energy Surface of the $F^- + CH_3CH_2Cl$ Reaction

Viktor Tajti and Gábor Czakó*

Department of Physical Chemistry and Materials Science, Institute of Chemistry, University of Szeged, Rerrich Béla tér 1, Szeged H-6720, Hungary

 Supporting Information

ABSTRACT: We compute benchmark structures, frequencies, and relative energies for the stationary points of the potential energy surface of the $F^- + CH_3CH_2Cl$ reaction using explicitly correlated ab initio levels of theory. CCSD(T)-F12b geometries and harmonic vibrational frequencies are obtained with the aug-cc-pVTZ and aug-cc-pVDZ basis sets, respectively. The benchmark relative energies are determined using a high-level composite method based on CCSD(T)-F12b/aug-cc-pVQZ frozen-core energies, CCSD(T)-F12b/cc-pCVTZ-F12 core electron correlation effects, and CCSD(T)-F12b/aug-cc-pVDZ zero-point energy corrections. The S_N2 channel leading to $Cl^- + CH_3CH_2F$ (−33.2) can proceed via back-side (−11.5), front-side (29.1), and double-inversion (18.0) transition states, whereas the bimolecular elimination (E2) products, $Cl^- + HF + C_2H_4$ (−19.3), can be formed via *anti* (−15.0) and *syn* (−7.3) saddle points, whose best adiabatic energies relative to $F^- + CH_3CH_2Cl$ are shown in parentheses in kcal/mol. Besides the S_N2 and E2 channels, the 0 K reaction enthalpies of the $HF + H_3C-CHCl^-$ (29.4), $H^- + H_3C-CHClF$ (46.2), $H^- + FH_2C-CH_2Cl$ (51.1), and $FCl^- + CH_3CH_2$ (49.7) product channels are determined. Utilizing the new benchmark data, the performance of the DF-MP2, MP2, MP2-F12, CCSD(T), and CCSD(T)-F12b methods with aug-cc-pVDZ and aug-cc-pVTZ basis sets is tested.



I. INTRODUCTION

The reactions of halide anions (X^-) with methyl-halides (CH_3Y) are important prototypes of the bimolecular nucleophilic substitution (S_N2) processes. Therefore, many experimental and theoretical studies have been recently focused on the $X^- + CH_3Y$ S_N2 reactions, thereby uncovering their complex dynamics.^{1–9} In 2016 Xie and Hase¹⁰ summarized the known atomic-level mechanisms of the gas-phase S_N2 reactions such as (a) rebound, (b) stripping, (c) front-side attack, (d) ion-dipole complex, (e) roundabout,² (f) hydrogen-bond complex, (g) front-side complex, and (h) double inversion.⁶ Mechanisms a–c are direct processes, and the others are indirect. Most of the above mechanisms proceed with inversion, known as Walden inversion,¹¹ except front-side attack and the recently discovered double inversion.⁶ The front-side attack retention pathway was already described in the early book of Ingold,¹² and the ab initio characterizations of the corresponding transition states (TSs) were reported decades ago.¹³ Recently, our reaction dynamics simulations on analytical potential energy surfaces allowed a quantitative analysis of the front-side attack S_N2 reactivity.^{6,7,9} Moreover, in 2015, the simulations revealed a double-inversion mechanism for the $F^- + CH_3Cl$ reaction,⁶ which was later found in the $F^- + CH_3F$ ⁷ and $F^- + CH_3I$ ⁹ reactions as well. The so-called double-inversion TSs were located and characterized for all the 16 possible $X^- + CH_3Y$ systems in 2015.¹⁴ Furthermore, in 2016, a double-inversion pathway was also described for the $F^- + CH_3Cl$ reaction in aqueous solution.¹⁵

One way to increase the complexity of the above-described S_N2 reactions is to replace CH_3Y with ethyl-halides (CH_3CH_2Y). Unlike in the case of the $X^- + CH_3Y$ reactions, for the $X^- + CH_3CH_2Y$ systems, besides the S_N2 channel ($Y^- + CH_3CH_2X$), a bimolecular elimination (E2) reaction leading to $Y^- + HX + C_2H_4$ can also occur. S_N2 and E2 are usually competing processes due to the close energetics of their reaction pathways. Most of the previous studies investigated the $X^- + CH_3CH_2X$ ($X = F, Cl$) identity reactions using density functional theory (DFT) and MP2 methods with double- and triple- ζ quality bases.^{16–18} In 2008, Bickelhaupt and co-workers¹⁹ reported CCSD(T) energy computations with basis sets up to aug-cc-pVQZ and aug-cc-pV(T+d)Z for $X = F$ and Cl , respectively. Among the nonidentity reactions, $F^- + CH_3CH_2Cl$ was studied using a modified G2(+) method,²⁰ and recently, $F^- + CH_3CH_2I$ was investigated based on MP2/ECP/d geometries and CCSD(T)/PP/t energies.²¹ These nonidentity reactions are of current experimental interest as well because Wester and co-workers have been studying the dynamics of various $X^- +$ alkyl-halide reactions, including $F^- + CH_3CH_2Cl$ and $F^- + CH_3CH_2I$.

In the present study, we focus on the $F^- + CH_3CH_2Cl$ reaction, extending our previous work^{5,6} on the $F^- + CH_3Cl$ system. As mention above, most of the earlier studies reported

Received: February 17, 2017

Revised: March 23, 2017

Published: March 24, 2017

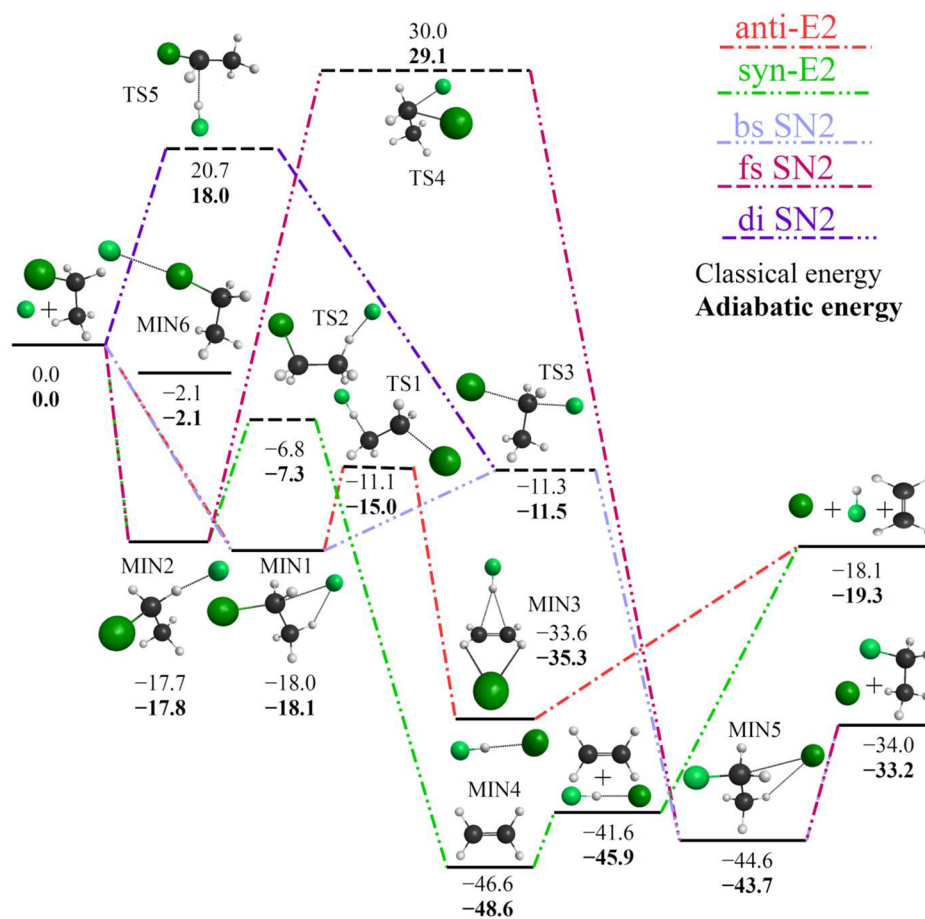


Figure 1. Schematic potential energy surface of the $F^- + CH_3CH_2Cl$ reaction showing the benchmark classical and adiabatic relative energies (kcal/mol) of the stationary points corresponding to the different reaction pathways. The classical energies are obtained at the CCSD(T)-F12b/aug-cc-pVQZ + $\Delta_{\text{core}}[\text{CCSD(T)-F12b/cc-pCVTZ-F12}]$ level of theory, and the adiabatic energies include $\Delta_{\text{ZPE}}[\text{CCSD(T)-F12b/aug-cc-pVDZ}]$ corrections as well.

DFT and MP2 results and in some cases standard CCSD(T) energies for the $X^- + CH_3CH_2Y$ systems.^{16–21} Here, we take advantage of the modern explicitly correlated CCSD(T)-F12b method²² to compute benchmark stationary-point structures, energetics, and frequencies for the title reaction. We consider basis sets up to aug-cc-pVQZ, core electron correlation effects, and zero-point vibrational energy corrections to determine the best technically feasible relative energies for various minima, transition states, and product channels on the complex potential energy surface of the $F^- + CH_3CH_2Cl$ reaction. On the basis of the new benchmark ab initio data, we test the performance of lower-level ab initio methods and basis sets. Furthermore, we investigate the existence of the above-mentioned double-inversion TS for $F^- + CH_3CH_2Cl$, which TS has not been determined for ethyl-halide systems so far. In Section II, the computational details are described. The results are presented in Section III, and the paper ends with summary and conclusions in Section IV.

II. COMPUTATIONAL DETAILS

The structures and harmonic vibrational frequencies of the stationary points are computed using the density-fitted second-order Møller–Plesset perturbation theory (DF-MP2),²³ standard MP2,²⁴ explicitly correlated MP2-F12,²⁵ standard coupled cluster with singles, doubles, and perturbative triples [CCSD(T)],²⁶ and explicitly correlated CCSD(T)-F12b²²

methods. For the open-shell systems (FCl^- and CH_3CH_2), restricted DF-RMP2, RMP2, and RMP2-F12 as well as unrestricted UCCSD(T) and UCCSD(T)-F12b methods are used based on restricted open-shell Hartree–Fock orbitals. All the electronic structure computations utilize the ab initio program package MOLPRO.²⁷

Geometry optimizations are performed with all the above methods using the correlation-consistent aug-cc-pVDZ and aug-cc-pVTZ basis sets.²⁸ Harmonic vibrational analyses are carried out using the aug-cc-pVDZ basis for all the methods, and the aug-cc-pVTZ basis is employed with DF-MP2, MP2, and MP2-F12. Thus, our best structures and frequencies are obtained at the CCSD(T)-F12b/aug-cc-pVTZ and CCSD(T)-F12b/aug-cc-pVDZ levels of theory, respectively. The interested reader can find all the computed results, including the definition of the internal coordinates in a Z-matrix representation, the structural parameters, harmonic frequencies, and absolute energies in the Supporting Information.

The benchmark classical relative energies are determined as

$$E[\text{CCSD(T)-F12b/aug-cc-pVQZ}] + \Delta_{\text{core}}[\text{CCSD(T)-F12b/cc-pCVTZ-F12}] \quad (1)$$

where E is the frozen-core energy and Δ_{core} is the core electron correlation correction obtained as difference between all-electron (correlating the valence and the $1s^2$ (C, F) and

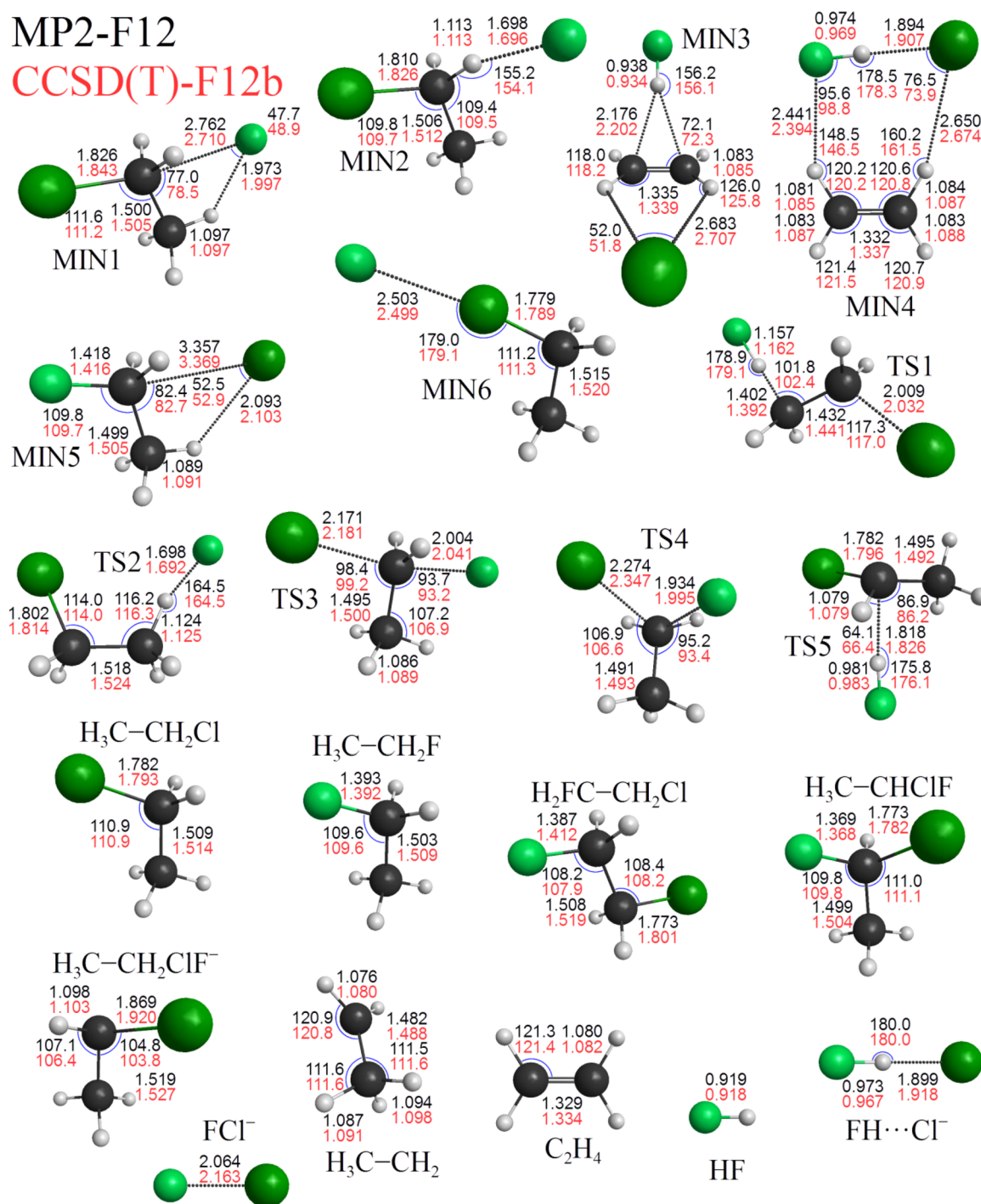


Figure 2. Structures of the stationary points showing the most important bond lengths (Å) and angles (degrees) obtained at the MP2-F12/aug-cc-pVTZ and CCSD(T)-F12b/aug-cc-pVTZ levels of theory.

$2s^22p^6$ (Cl) core electrons) and frozen-core (correlating the valence electrons only) energies at the CCSD(T)-F12b/aug-cc-pVTZ geometries.

Finally, the best adiabatic relative energies are obtained as

$$\begin{aligned}
 & E[\text{CCSD(T)-F12b/aug-cc-pVQZ}] \\
 & + \Delta\text{core}[\text{CCSD(T)-F12b/cc-pCVTZ-F12}] \\
 & + \Delta\text{ZPE}[\text{CCSD(T)-F12b/aug-cc-pVDZ}] \quad (2)
 \end{aligned}$$

where ΔZPE is the zero-point energy correction.

III. RESULTS AND DISCUSSION

The benchmark potential energy diagram for the different $\text{S}_{\text{N}}2$ and E2 pathways of the $\text{F}^- + \text{CH}_3\text{CH}_2\text{Cl}$ reaction is shown in Figure 1. Both the $\text{S}_{\text{N}}2$ and E2 processes are exothermic with ΔH_0 values of -33.2 and -19.3 kcal/mol, respectively. Because the $\text{S}_{\text{N}}2$ channel is more exothermic than E2, the $\text{S}_{\text{N}}2$ products are clearly favored under simple thermodynamic control. However, considering the relative energies of stationary points along the reaction pathways, a different picture emerges. As shown in Figure 1, the $\text{S}_{\text{N}}2$ products can be obtained by the back-side (bs) attack mechanism via a reactant-like ion-dipole

Table 1. Classical and Adiabatic (in Parenthesis) Relative Energies (in kcal/mol, with Respect to the Reactants) Of the Various Minima, Transition States (Figure 1), and Product Channels on the Potential Energy Surface of the $F^- + CH_3CH_2Cl$ Reaction at Different Levels of Theory

basis method	aug-cc-pVDZ					aug-cc-pVTZ				
	DF-MP2	MP2	MP2-F12	CCSD(T)	CCSD(T)-F12b	DF-MP2	MP2	MP2-F12	CCSD(T) ^a	CCSD(T)-F12b ^a
MIN1	-17.8	-17.8	-17.7	-18.7	-18.5	-17.5	-17.5	-17.4	-18.4	-18.3
	(-17.8)	(-17.8)	(-17.7)	(-18.7)	(-18.5)	(-17.5)	(-18.4)	(-17.1)	(-18.3)	(-18.4)
MIN2	-17.5	-17.5	-17.5	-18.4	-18.1	-17.3	-17.3	-17.2	-18.0	-17.9
	(-17.7)	(-17.7)	(-17.7)	(-18.4)	(-18.3)	(-17.4)	(-17.4)	(-17.4)	(-18.1)	(-18.1)
MIN3	-31.8	-31.8	-30.9	-33.8	-33.6	-30.6	-30.6	-30.6	-33.2	-33.4
	(-33.8)	(-33.8)	(-32.8)	(-35.9)	(-35.3)	(-32.8)	(-32.8)	(-32.6)	(-35.2)	(-35.2)
MIN4	-44.2	-44.2	-43.5	-46.4	-46.4	-43.7	-43.7	-43.4	-46.5	-46.4
	(-46.3)	(-46.3)	(-45.7)	(-48.2)	(-48.4)	(-46.0)	(-46.0)	(-45.6)	(-48.3)	(-48.4)
MIN5	-42.4	-42.4	-41.8	-44.8	-44.7	-41.6	-41.5	-41.5	-44.5	-44.8
	(-41.3)	(-41.3)	(-40.9)	(-43.7)	(-43.8)	(-40.5)	(-40.5)	(-40.9)	(-43.4)	(-43.8)
MIN6	-0.8	-0.8	-2.6 ^b	-1.5	-3.1 ^b	-1.4	-1.4	-1.8	-1.9	-2.4
	(-0.7)	(-0.7)	(-2.4) ^b	(-1.4)	(-3.0) ^b	(-1.3)	(-1.3)	(-1.8)	(-1.8)	(-2.3)
TS1	-11.3	-11.2	-10.9	-12.0	-11.4	-11.3	-11.3	-10.8	-11.9	-11.4
	(-15.2)	(-15.2)	(-14.8)	(-15.9)	(-15.3)	(-15.2)	(-15.2)	(-14.8)	(-15.9)	(-15.3)
TS2	-6.4	-6.4	-6.6	-7.4	-7.3	-6.2	-6.2	-6.2	-7.1	-7.1
	(-6.9)	(-6.9)	(-7.1)	(-7.8)	(-7.8)	(-6.8)	(-6.8)	(-6.7)	(-7.6)	(-7.6)
TS3	-11.0	-11.0	-8.8	-13.9	-11.4	-9.4	-9.4	-8.9	-12.4	-11.8
	(-11.1)	(-11.1)	(-9.0)	(-14.1)	(-11.6)	(-9.5)	(-9.5)	(-8.9)	(-12.5)	(-12.0)
TS4	31.0	31.1	32.6	26.9	29.4	32.6	32.6	32.9	28.7	29.3
	(30.3)	(30.3)	(32.0)	(26.1)	(28.5)	(31.7)	(31.8)	(32.1)	(27.8)	(28.5)
TS5	23.7	23.8	20.5	23.1	19.9	21.3	21.3	20.8	21.0	20.4
	(20.7)	(20.7)	(17.6)	(20.1)	(17.2)	(18.4)	(18.4)	(17.9)	(18.0)	(17.6)
Cl ⁻ + CH ₃ CH ₂ F	-31.3	-31.3	-30.8	-33.6	-33.8	-30.7	-30.6	-30.8	-33.7	-34.1
	(-30.4)	(-30.4)	(-29.9)	(-32.8)	(-33.0)	(-29.8)	(-29.8)	(-29.8)	(-32.8)	(-33.3)
FH...Cl ⁻ + C ₂ H ₄	-38.6	-38.6	-37.9	-40.6	-40.7	-38.3	-38.3	-38.3	-41.1	-41.3
	(-43.0)	(-43.0)	(-42.5)	(-44.8)	(-45.1)	(-42.8)	(-42.8)	(-42.7)	(-45.3)	(-45.6)
Cl ⁻ + HF + C ₂ H ₄	-15.5	-15.5	-13.9	-17.8	-17.1	-14.1	-14.1	-14.4	-17.2	-17.7
	(-16.7)	(-16.7)	(-15.3)	(-19.0)	(-18.4)	(-15.6)	(-15.6)	(-15.7)	(-18.4)	(-18.9)
HF + H ₃ C-CHCl ⁻	34.0	34.0	33.0	30.8	30.2	32.7	32.7	32.6	30.3	30.2
	(32.6)	(32.6)	(31.7)	(29.4)	(28.9)	(31.4)	(31.4)	(31.9)	(28.9)	(28.9)
H ⁻ + H ₃ C-CHClF	57.8	57.7	56.0	50.9	48.5	56.5	56.4	56.9	50.2	50.2
	(52.9)	(52.8)	(51.0)	(46.1)	(43.7)	(51.6)	(51.5)	(52.0)	(45.4)	(45.3)
H ⁻ +FH ₂ C-CH ₂ Cl	62.3	62.2	60.9	55.0	53.1	61.2	61.1	61.7	54.5	54.6
	(57.9)	(57.9)	(56.6)	(50.7)	(48.9)	(56.8)	(56.7)	(57.3)	(50.2)	(50.4)
FCI ⁻ + CH ₃ CH ₂	53.7	53.7	58.3	49.7	53.3	56.6	56.7	57.9	52.9	53.8
	(51.4)	(51.4)	(55.5)	(45.1)	(48.8)	(54.0)	(54.1)	(55.1)	(48.4)	(49.2)

^aFor the CCSD(T) and CCSD(T)-F12b adiabatic energies, the ZPE corrections are obtained with the aug-cc-pVDZ basis. ^bThese data correspond to a first-order saddle point (see Table S6 for more details).

complex (-18.0/-18.1), Walden-inversion TS (-11.3/-11.5), and product-like ion-dipole complex (-44.6/-43.7), whose classical/adiabatic energies in kcal/mol relative to the reactants are given in parentheses. For the elimination reaction, we can distinguish between *anti*-E2 and *syn*-E2 mechanisms. The *anti*-E2 pathway goes through the same ion-dipole complex (-18.0/-18.1) as the *bs*-S_N2 pathway; then over an *anti*-[Cl...CH₂CH₂...HF]⁻ TS (-11.1/-15.0), and finally, the products are formed via a Cl⁻...C₂H₄...HF complex (-33.6/-35.3). As seen, the classical barriers for the *bs*-S_N2 and *anti*-E2 pathways are similar, 6.7 and 6.9 kcal/mol, relative to the ion-dipole minimum, respectively. Considering the ZPE effects, the *bs*-S_N2 barrier is only slightly affected as it becomes 6.6 kcal/mol, whereas the *anti*-E2 barrier significantly reduces to 3.1 kcal/mol. Thus, while the classical barrier is slightly larger for the *anti*-E2 channel, the vibrationally adiabatic *anti*-E2 barrier height is less than half that of the *bs*-S_N2 barrier. This means that, unlike the thermodynamic control, kinetic control

suggests higher reactivity for the E2 reaction, and the ZPE effect plays a key role in this prediction. The *syn*-E2 pathway goes through a hydrogen-bonded prereaction complex (-17.7/-17.8), followed by a *syn*-[ClCH₂CH₂H...F]⁻ TS (-6.8/-7.3) and a (Cl⁻...HF)...C₂H₄ complex (-46.6/-48.6), which dissociates to Cl⁻...HF + C₂H₄ (-41.6/-45.9) and finally gives Cl⁻ + HF + C₂H₄ (-18.1/-19.3). As indicated in parentheses, the hydrogen-bonded minimum has energy similar to that of the ion-dipole complex. Interestingly, here, the ion-dipole minimum is slightly deeper by 0.3 kcal/mol, whereas in the case of the F⁻ + CH₃Cl and F⁻ + CH₃CH₂I reactions, the hydrogen-bonded complexes were found deeper by 1.3 and 0.5 kcal/mol, respectively.^{6,21} The *syn*-E2 TS is above the prereaction minimum by 10.9/10.5 kcal/mol; thus, the barrier for *syn*-E2 is significantly higher than that of the *anti*-E2 pathway. The (Cl⁻...HF)...C₂H₄ complex is found to be the global minimum of the complex potential energy surface. Examining the structures shown in Figure 2, one can observe that the *anti*-

Table 2. Benchmark Classical and Adiabatic Relative Energies (in kcal/mol, with Respect to the Reactants) Of the Various Minima, Transition States (Figure 1), and Product Channels on the Potential Energy Surface of the $F^- + CH_3CH_2Cl$ Reaction

stationary point	aVQZ ^a	Δ core ^b	Δ ZPE ^c	classical ^d	adiabatic ^e
MIN1	-18.1	0.1	-0.0	-18.0	-18.1
MIN2	-17.7	0.0	-0.2	-17.7	-17.8
MIN3	-33.5	-0.0	-1.7	-33.6	-35.3
MIN4	-46.5	-0.1	-1.9	-46.6	-48.6
MIN5	-44.8	0.2	1.0	-44.6	-43.7
MIN6	-2.2	0.0	0.1	-2.1	-2.1
TS1	-11.2	0.1	-3.9	-11.1	-15.0
TS2	-6.9	0.0	-0.5	-6.8	-7.3
TS3	-11.6	0.4	-0.2	-11.3	-11.5
TS4	29.6	0.4	-0.8	30.0	29.1
TS5	20.7	0.1	-2.8	20.7	18.0
$Cl^- + CH_3CH_2F$	-34.2	0.2	0.9	-34.0	-33.2
$FH \cdots Cl^- + C_2H_4$	-41.5	-0.1	-4.3	-41.6	-45.9
$Cl^- + HF + C_2H_4$	-18.1	0.0	-1.2	-18.1	-19.3
$HF + H_3C-CHCl^-$	30.3	0.4	-1.3	30.7	29.4
$H^- + H_3C-CHClF$	50.8	0.2	-4.8	51.0	46.2
$H^- + FH_2C-CH_2Cl$	55.2	0.2	-4.2	55.4	51.1
$FCl^- + CH_3CH_2$	53.9	0.2	-4.5	54.2	49.7

^aFrozen-core energies obtained at the CCSD(T)-F12b/aug-cc-pVQZ level of theory at CCSD(T)-F12b/aug-cc-pVTZ geometries. ^bCore correlation effects obtained as differences between all-electron and frozen-core energies at the CCSD(T)-F12b/cc-pCVTZ-F12 level of theory at CCSD(T)-F12b/aug-cc-pVTZ geometries. ^cHarmonic zero-point energy corrections at the CCSD(T)-F12b/aug-cc-pVDZ level of theory. ^dBenchmark classical relative energies obtained as CCSD(T)-F12b/aug-cc-pVQZ + Δ core. ^eBenchmark adiabatic relative energies obtained as CCSD(T)-F12b/aug-cc-pVQZ + Δ core + Δ ZPE.

(TS1) and *syn*-E2 (TS2) transition states differ not just in their conformations. In the TS1 the C–Cl and C–H bonds are stretched by 0.239 and 0.300 Å, respectively, relative to the corresponding bond lengths in CH_3CH_2Cl , and the H–F distance is 1.162 Å. TS2 is more reactant-like because the C–Cl and C–H distances are just 0.021 and 0.033 Å longer than those in the reactant, and the H–F distance is as long as 1.692 Å.

Besides the back-side attack Walden-inversion S_N2 pathway, a front-side attack retention mechanism also exists via a high-energy barrier (30.0/29.1 kcal/mol), as also shown in Figure 1. At the front-side attack transition state (TS4), both F and Cl connect to the same C atom, where the dissociating C–Cl and forming C–F distances are 2.347 and 1.995 Å, whereas the corresponding bond lengths are 1.793 and 1.392 Å in the reactant and product, respectively, as shown in Figure 2. Motivated by our previous findings on the $F^- +$ methyl-halide systems,^{6,7,9,14} we also investigated whether double inversion can occur in the $F^- + CH_3CH_2Cl$ reaction. We found a double-inversion transition state (TS5) for the title reaction, where an FH connects to $[CHCl-CH_3]^-$, while the $CHCl-C$ unit is almost planar. The double-inversion barrier height (20.7/18.0 kcal/mol) is well below the front-side attack TS. The relative energies and structures of the above-discussed TS4 and TS5 are qualitatively similar to those of the corresponding TSs of the $F^- + CH_3Cl$ reaction. The front-side attack barrier height of the title reaction is only below the barrier of $F^- + CH_3Cl$ by about 1 kcal/mol, whereas the present double-inversion TS is above the corresponding $F^- + CH_3Cl$ TS by about 5 kcal/mol.⁶ In both cases, double inversion is the lower-energy retention pathway. For TS4, the C–F and C–Cl distances of 1.995 and 2.347 Å, respectively, are very similar to the corresponding values of 1.910 and 2.319 Å found previously for the front-side TS of $F^- + CH_3Cl$ at the same CCSD(T)-F12b/aug-cc-pVTZ level of theory.¹⁴ Furthermore, as seen in Figure 2, for TS5, the

F–H and H \cdots C distances are 0.983 and 1.826 Å, respectively, which are only slightly different from the corresponding 0.988 and 1.807 Å values of double-inversion TS of the $F^- + CH_3Cl$ reaction.¹⁴

In the entrance channel, we found a weakly bound complex (MIN6) with $F^- \cdots ClCH_2CH_3$ nonreactive orientation, in which F^- connects to the Cl atom. The $F^- \cdots Cl-C$ arrangement is almost collinear (179.1°), and the $F^- \cdots Cl$ equilibrium distance is 2.499 Å, as shown in Figure 2. The energy of MIN6 is just slightly below the reactant asymptote by 2.1 kcal/mol; thus, this complex may not steer the reactants away from the reactive orientations. A similar front-side complex was found for $F^- \cdots ClCH_3$ with dissociation energy of 3.1 kcal/mol,⁸ whereas the corresponding $F^- \cdots ICH_3$ complex belongs to a deep minimum below the reactants by 22.1 kcal/mol.⁹ These complexes were predicted to play a key role in the difference of the dynamics of the $F^- + CH_3Cl$ and $F^- + CH_3I$ reactions, and the similar complexes may become important in the $F^- +$ ethyl-halide reactions as well.

The classical and adiabatic relative energies obtained by DF-MP2, MP2, MP2-F12, CCSD(T), and CCSD(T)-F12b with the aug-cc-pVDZ and aug-cc-pVTZ basis sets are given in Table 1, and the final benchmark energies are presented in Table 2. Besides the stationary points corresponding to the above-discussed S_N2 and E2 reactions, the reaction enthalpies of additional higher-energy product channels such as the proton abstraction ($HF + H_3C-CHCl^-$), hydrogen substitution ($H^- + H_3C-CHClF$ and $H^- + FH_2C-CH_2Cl$), and halogen abstraction ($FCl^- + CH_3CH_2$) are also given in Tables 1 and 2. These reaction channels are all endothermic, with benchmark classical/adiabatic energies of 30.7/29.4, 51.0/46.2, 55.4/51.1, and 54.2/49.7 kcal/mol, in the above order. For the proton abstraction reaction, one can imagine two channels leading to either $HF + H_3C-CHCl^-$ or $HF + H_2C-CH_2Cl$. We found only the former because we could not locate a stable structure

for $\text{H}_2\text{C}^- - \text{CH}_2\text{Cl}$ using the above-defined levels of theory. The hydrogen substitution, i.e., F^- and H^- exchange, is found to be thermodynamically favored on the C^α atom to which Cl is connected because the energy of $\text{H}_3\text{C}^\beta - \text{C}^\alpha\text{HClF}$ is deeper by 4.9 kcal/mol than that of $\text{FH}_2\text{C}^\beta - \text{C}^\alpha\text{H}_2\text{Cl}$. This finding is in accord with the fact that, due to the polar $\text{C}^\alpha - \text{Cl}$ bond, the C^α atom of $\text{H}_3\text{C}^\beta - \text{C}^\alpha\text{H}_2\text{Cl}$ is more electrophile than C^β ; thus, the nucleophilic attack is more likely on C^α .

As Table 1 shows, the DF-MP2 relative energies agree with the standard MP2 values within 0.1 kcal/mol. The explicitly correlated F12 methods clearly show better convergence with increasing basis size. For example, for TS4, the standard MP2[CCSD(T)] gives classical barrier heights of 31.1[26.9] and 32.6[28.7] kcal/mol with aug-cc-pVDZ and aug-cc-pVTZ, respectively, whereas MP2-F12[CCSD(T)-F12b] provides 32.6[29.4] and 32.9[29.3] kcal/mol, in order. As also seen in the above example, MP2 usually overestimates the CCSD(T) energies by 1–4 kcal/mol for the minima and transition states, and even larger deviations of 2–8 kcal/mol are found for the product channels. The performance of the various methods and basis sets is further analyzed in Figures 3–5. The root-mean-

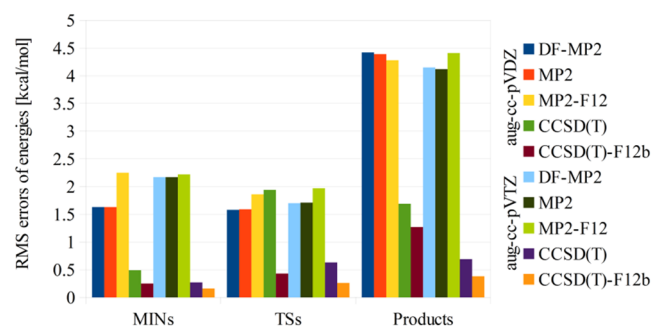


Figure 3. RMS deviations of the relative energies of the minima (MINs), transition states (TSs), and products obtained at different levels of theory relative to the CCSD(T)-F12b/aug-cc-pVQZ reference data.

square (RMS) deviations between the relative energies obtained at different levels of theory and the CCSD(T)-F12b/aug-cc-pVQZ values are shown in Figure 3. As seen, the MP2 methods give RMS errors of about 1.5–2.5, 1.5–2, and 4–4.5 kcal/mol for the minima, transition states, and products, respectively, independently of the basis set. Thus, MP2 does not provide chemical accuracy, which is defined as accuracy within 1 kcal/mol, for the relative energies of the title reaction. The standard CCSD(T) method with the aug-cc-pVDZ basis

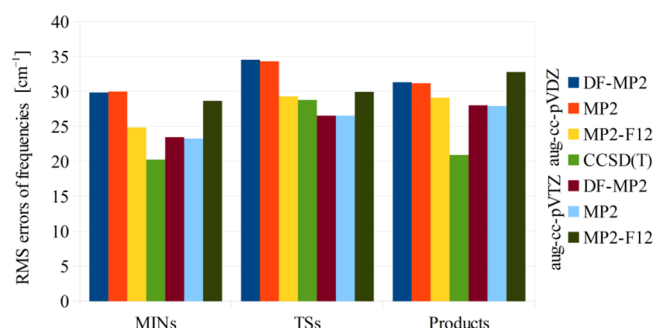


Figure 5. RMS deviations of the frequencies of the minima (MINs), transition states (TSs), and products obtained at different levels of theory relative to the CCSD(T)-F12b/aug-cc-pVDZ reference data.

provides chemical accuracy for the minima, but for the TSs and products, 1.5–2 kcal/mol RMS error is seen. The F12 method decreases this error below 0.5 and 1.5 kcal/mol for the TSs and products, respectively. Using the aug-cc-pVTZ basis, the standard CCSD(T) energies significantly improve resulting in 0.3, 0.6, and 0.7 RMS errors, for the minima, TSs, and products, respectively. The CCSD(T)-F12b results are even more accurate because all the RMS errors are below 0.5 kcal/mol, i.e., 0.2, 0.3, and 0.4 kcal/mol, in the above order.

All of the bond lengths, bond angles, and dihedral angles of the stationary points obtained at different levels of theory are given in the Tables S1–S21 in the Supporting Information. The RMS errors of these structural parameters relative to the new benchmark CCSD(T)-F12b/aug-cc-pVTZ results are shown in Figure 4 and in more detail in Table S23. The MP2 methods with the aug-cc-pVDZ basis give average accuracies of about 0.02 Å, 0.5–1°, and 1–2° for the bond lengths, bond angles, and dihedral angles, respectively (note that the angles are more accurate for the products). This does not significantly improve if we increase the basis size to aug-cc-pVTZ. The standard CCSD(T) method with the aug-cc-pVDZ basis provides similar or in some cases even larger RMS errors as the MP2 methods. The F12 approach significantly improves the CCSD(T)/aug-cc-pVDZ geometries and provides an accuracy comparable to or for the distances even better than the standard CCSD(T)/aug-cc-pVTZ results, which agree with the benchmark reference data within about 0.005 Å, 0.2°, and 0.2° for the distances, bond angles, and dihedral angles, in order.

The RMS errors of the harmonic vibrational frequencies obtained with different methods and basis sets relative to the benchmark CCSD(T)-F12b/aug-cc-pVDZ results are shown in Figure 5. As seen, the DF-MP2 and MP2 methods give virtually

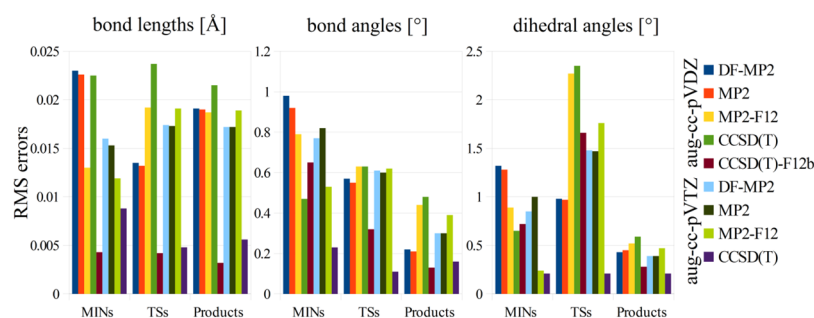


Figure 4. RMS deviations of the structural parameters of the minima (MINs), transition states (TSs), and products obtained at different levels of theory relative to the CCSD(T)-F12b/aug-cc-pVTZ reference data.

the same frequencies with an average accuracy of about 30 cm^{-1} with the aug-cc-pVDZ basis, and only a few cm^{-1} improvement is found with the aug-cc-pVTZ basis. The CCSD(T)/aug-cc-pVDZ frequencies are slightly better than the MP2 values and agree with the reference data within about $20\text{--}25\text{ cm}^{-1}$ for the minima and products and within $25\text{--}30\text{ cm}^{-1}$ for the TSs. Overall, in the case of the title reaction, we find that all the present methods and basis sets provide similar frequencies with an accuracy of $20\text{--}35\text{ cm}^{-1}$ ($0.06\text{--}0.10\text{ kcal/mol}$).

Besides the benchmark energies their components such as the CCSD(T)-F12b/aug-cc-pVQZ energies, the core electron correlation effects and ZPE corrections are given in Table 2. As Figure 3 shows, the CCSD(T)-F12b energies with the aug-cc-pVTZ and aug-cc-pVQZ basis sets agree within about 0.3 kcal/mol on average; thus, knowing the fast basis-set convergence of the F12 methods, we can predict an average accuracy of 0.1 kcal/mol with respect to the complete basis set limit for the present CCSD(T)-F12b/aug-cc-pVQZ relative energies. Note that uncertainties of the geometries are likely to result in negligible effects on the relative energies. To prove this, we performed CCSD(T)-F12b optimizations with the aug-cc-pVQZ basis for $\text{CH}_3\text{CH}_2\text{F}$ and $\text{CH}_3\text{CH}_2\text{Cl}$. The CCSD(T)-F12b/aug-cc-pVQZ $\text{S}_{\text{N}}2$ reaction energies at the aug-cc-pVTZ and aug-cc-pVQZ geometries are found to agree within $\sim 0.00004\text{ kcal/mol}$ (numerical noise level); thus, it is not worth (and in some cases not feasible) computing the geometries with the aug-cc-pVQZ basis. Core correlation effects are small and usually increase the relative energies by $0.0\text{--}0.4\text{ kcal/mol}$. The ZPE corrections are significant and in most cases decrease the relative energies by $0\text{--}5\text{ kcal/mol}$. Besides the negligible ZPE effect of $+0.1\text{ kcal/mol}$ of the weakly bound MIN6 complex, the two cases where positive ZPE effects, 1.0 and 0.9 kcal/mol , are seen are the MIN5 product-type complex and the $\text{Cl}^- + \text{CH}_3\text{CH}_2\text{F}$ product channel, respectively, due to the fact that $\text{CH}_3\text{CH}_2\text{F}$ has ZPE larger than that of $\text{CH}_3\text{CH}_2\text{Cl}$. The most significant ZPE effects are found for TS1 (-3.9 kcal/mol), lowering the transition-state region of the *anti*-E2 reaction path below the *bs*- $\text{S}_{\text{N}}2$ TS3 as discussed earlier and for the double-inversion TS5 (-2.8 kcal/mol). Furthermore, the ZPE corrections (between -4 and -5 kcal/mol) are even larger for some of the product channels, as seen in Table 2. The three remaining auxiliary energy contributions which are not considered in the present study are the relativistic effects, the post-CCSD(T) correlation contributions, and the anharmonic corrections to the frequencies. On the basis of our previous studies,^{6,7,29} the relativistic effects are likely to be less than 0.1 kcal/mol and are certainly below the core correlation effects. The post-CCSD(T) corrections are expected to be between 0.0 and 0.3 kcal/mol , and the largest corrections could be predicted for the TSs, especially for the front-side TS4, where the effect can be as large as 0.5 kcal/mol (see ref 7, where we reported -0.54 kcal/mol for the front-side TS of $\text{F}^- + \text{CH}_3\text{F}$). The anharmonic effects on the ZPE corrections are usually 5% of the harmonic values, which are between 0.0 and 0.2 kcal/mol in the present case.

IV. SUMMARY AND CONCLUSIONS

We reported a high-level *ab initio* characterization of the potential energy surface (PES) of the title reaction. The explicitly correlated CCSD(T)-F12b computations provide benchmark stationary-point structures, frequencies, and relative energies for the $\text{F}^- + \text{CH}_3\text{CH}_2\text{Cl}$ system and set new state of the art computations for $\text{S}_{\text{N}}2$ reactions of ethyl-halides.

Furthermore, the new chemically accurate benchmark results allow testing different lower levels of theory, showing that the MP2 methods usually provide uncertainties of $1.5\text{--}2.5\text{ kcal/mol}$ and even larger ones of $4.0\text{--}4.5\text{ kcal/mol}$ for the high-energy product channels.

We found that the transition states of the back-side $\text{S}_{\text{N}}2$ and *anti*-E2 pathways have the same classical energy within 0.2 kcal/mol , whereas the ZPE correction lowers the *anti*-E2 TS below the *bs*- $\text{S}_{\text{N}}2$ TS by 3.5 kcal/mol . Thus, on a vibrationally adiabatic PES, the *anti*-E2 mechanism is kinetically favored, whereas the more exothermic $\text{S}_{\text{N}}2$ channel is expected to dominate under thermodynamic control. We found a double-inversion TS for the title reaction, which was previously described for $\text{S}_{\text{N}}2$ reactions of methyl-halides^{6,14} but reported for the first time for an ethyl-halide reaction. The adiabatic barrier height of the double-inversion pathway is 18.0 kcal/mol , well below the front-side attack $\text{S}_{\text{N}}2$ barrier of 29.1 kcal/mol . To theoretically investigate the role of the above-mentioned $\text{S}_{\text{N}}2$ and E2 mechanisms and support the ongoing crossed-beam experiments, reaction dynamics simulations are desired. Therefore, in the near future, we plan to develop a global analytical PES for the title reaction. The present high-level *ab initio* study of the stationary points is an important first step toward the above-mentioned PES. The development of a global PES requires the knowledge of the energetics of the different product asymptotes of the reactive system, which is the reason why we investigated the various high-energy product channels such as $\text{HF} + \text{H}_3\text{C}-\text{CHCl}^-$, $\text{H}^- + \text{H}_3\text{C}-\text{CHClF}$, $\text{H}^- + \text{FH}_2\text{C}-\text{CH}_2\text{Cl}$, and $\text{FCl}^- + \text{CH}_3\text{CH}_2$. A detailed study of the mechanisms of the above endothermic reaction channels is also an interesting future research direction. The present results and definitive predictions can provide guidance for experimental studies, analytic global PES developments, and dynamics simulations of the title reaction as well as for *ab initio* investigations of similar systems.

■ ASSOCIATED CONTENT

Supporting Information

The Supporting Information is available free of charge on the ACS Publications website at DOI: 10.1021/acs.jpca.7b01572.

Energies, structural parameters, harmonic vibrational frequencies, and RMS errors of the bond lengths, bond angles, and dihedral angles for all the stationary points at different levels of theory (PDF)

■ AUTHOR INFORMATION

Corresponding Author

*E-mail: gczako@chem.u-szeged.hu.

ORCID

Gábor Czako: 0000-0001-5136-4777

Notes

The authors declare no competing financial interest.

■ ACKNOWLEDGMENTS

G.C. thanks the Scientific Research Fund of Hungary (Grant PD-111900) and the János Bolyai Research Scholarship of the Hungarian Academy of Sciences for financial support. We acknowledge the National Information Infrastructure Development Institute for awarding us access to resource based in Hungary at Debrecen and Szeged.

REFERENCES

- (1) Brauman, J. I. Not So Simple. *Science* **2008**, *319*, 168–168.
- (2) Mikosch, J.; Trippel, S.; Eichhorn, C.; Otto, R.; Lourderaj, U.; Zhang, J.-X.; Hase, W. L.; Weidemüller, M.; Wester, R. Imaging Nucleophilic Substitution Dynamics. *Science* **2008**, *319*, 183–186.
- (3) Manikandan, P.; Zhang, J.; Hase, W. L. Chemical Dynamics Simulations of $X^- + CH_3Y \rightarrow XCH_3 + Y^-$ Gas-Phase S_N2 Nucleophilic Substitution Reactions. Nonstatistical Dynamics and Nontraditional Reaction Mechanisms. *J. Phys. Chem. A* **2012**, *116*, 3061–3080.
- (4) Xie, J.; Otto, R.; Mikosch, J.; Zhang, J.; Wester, R.; Hase, W. L. Identification of Atomic-Level Mechanisms for Gas-Phase $X^- + CH_3Y$ S_N2 Reactions by Combined Experiments and Simulations. *Acc. Chem. Res.* **2014**, *47*, 2960–2969.
- (5) Szabó, I.; Császár, A. G.; Czakó, G. Dynamics of the $F^- + CH_3Cl \rightarrow Cl^- + CH_3F$ S_N2 Reaction on a Chemically Accurate Potential Energy Surface. *Chem. Sci.* **2013**, *4*, 4362–4370.
- (6) Szabó, I.; Czakó, G. Revealing a Double-Inversion Mechanism for the $F^- + CH_3Cl$ S_N2 Reaction. *Nat. Commun.* **2015**, *6*, 5972.
- (7) Szabó, I.; Telekes, H.; Czakó, G. Accurate ab Initio Potential Energy Surface, Thermochemistry, and Dynamics of the $F^- + CH_3F$ S_N2 and Proton-Abstraction Reactions. *J. Chem. Phys.* **2015**, *142*, 244301.
- (8) Stei, M.; Carrascosa, E.; Kainz, M. A.; Kelkar, A. H.; Meyer, J.; Szabó, I.; Czakó, G.; Wester, R. Influence of the Leaving Group on the Dynamics of a Gas-Phase S_N2 Reaction. *Nat. Chem.* **2016**, *8*, 151–156.
- (9) Olasz, B.; Szabó, I.; Czakó, G. High-Level ab Initio Potential Energy Surface and Dynamics of the $F^- + CH_3I$ S_N2 and Proton-Transfer Reactions. *Chem. Sci.* **2017**, *8*, 3164–3170.
- (10) Xie, J.; Hase, W. L. Rethinking the S_N2 Reaction. *Science* **2016**, *352*, 32–33.
- (11) Walden, P. Ueber die Gegenseitige Umwandlung Optischer Antipoden. *Ber. Dtsch. Chem. Ges.* **1896**, *29*, 133–138.
- (12) Ingold, C. K. *Structure and Mechanisms in Organic Chemistry*; Cornell University Press: Ithaca, NY, 1953.
- (13) Glukhovtsev, M. N.; Pross, A.; Schlegel, H. B.; Bach, R. D.; Radom, L. Gas-Phase Identity S_N2 Reactions of Halide Anions and Methyl Halides with Retention of Configuration. *J. Am. Chem. Soc.* **1996**, *118*, 11258–11264.
- (14) Szabó, I.; Czakó, G. Double-Inversion Mechanisms of the $X^- + CH_3Y$ [$X, Y = F, Cl, Br, I$] S_N2 Reactions. *J. Phys. Chem. A* **2015**, *119*, 3134–3140.
- (15) Liu, P.; Wang, D. Y.; Xu, Y. A New, Double-Inversion Mechanism of the $F^- + CH_3Cl$ S_N2 Reaction in Aqueous Solution. *Phys. Chem. Chem. Phys.* **2016**, *18*, 31895–31903.
- (16) Bickelhaupt, F. M.; Baerends, E. J.; Nibbering, N. M. M.; Ziegler, T. Theoretical Investigation on Base-Induced 1,2-Eliminations in the Model System $F^- + CH_3CH_2F$. The Role of the Base as a Catalyst. *J. Am. Chem. Soc.* **1993**, *115*, 9160–9173.
- (17) Bickelhaupt, F. M. Understanding Reactivity with Kohn–Sham Molecular Orbital Theory: E2- S_N2 Mechanistic Spectrum and Other Concepts. *J. Comput. Chem.* **1999**, *20*, 114–128.
- (18) Ensing, B.; Klein, M. L. Perspective on the Reactions Between F^- and CH_3CH_2F : The Free Energy Landscape of the E2 and S_N2 Reaction Channels. *Proc. Natl. Acad. Sci. U. S. A.* **2005**, *102*, 6755–6759.
- (19) Bento, A. P.; Solà, M.; Bickelhaupt, F. M. E2 and S_N2 Reactions of $X^- + CH_3CH_2X$ ($X = F, Cl$); an ab Initio and DFT Benchmark Study. *J. Chem. Theory Comput.* **2008**, *4*, 929–940.
- (20) Wu, X.-P.; Sun, X.-M.; Wei, X.-G.; Ren, Y.; Wong, N.-B.; Li, W.-K. Exploring the Reactivity Trends in the E2 and S_N2 Reactions of $X^- + CH_3CH_2Cl$ ($X = F, Cl, Br, HO, HS, HSe, NH_2, PH_2, AsH_2, CH_3, SiH_3, \text{ and } GeH_3$). *J. Chem. Theory Comput.* **2009**, *5*, 1597–1606.
- (21) Yang, L.; Zhang, J.; Xie, J.; Ma, X.; Zhang, L.; Zhao, C.; Hase, W. L. Competing E2 and S_N2 Mechanisms for the $F^- + CH_3CH_2I$ Reaction. *J. Phys. Chem. A* **2017**, *121*, 1078–1085.
- (22) Adler, T. B.; Knizia, G.; Werner, H.-J. A Simple and Efficient CCSD(T)-F12 Approximation. *J. Chem. Phys.* **2007**, *127*, 221106.
- (23) Werner, H.-J.; Manby, F. R.; Knowles, P. J. Fast Linear Scaling Second-Order Møller-Plesset Perturbation Theory (MP2) Using Local and Density Fitting Approximations. *J. Chem. Phys.* **2003**, *118*, 8149–8160.
- (24) Møller, C.; Plesset, M. S. Note on an Approximation Treatment for Many-Electron Systems. *Phys. Rev.* **1934**, *46*, 618–622.
- (25) Werner, H.-J.; Adler, T. B.; Manby, F. R. General Orbital Invariant MP2-F12 Theory. *J. Chem. Phys.* **2007**, *126*, 164102.
- (26) Raghavachari, K.; Trucks, G. W.; Pople, J. A.; Head-Gordon, M. A Fifth-Order Perturbation Comparison of Electron Correlation Theories. *Chem. Phys. Lett.* **1989**, *157*, 479–483.
- (27) Werner, H.-J.; Knowles, P. J.; Knizia, G.; Manby, F. R.; Schütz, M. MOLPRO, version 2015.1, a package of ab initio programs. <http://www.molpro.net> (accessed March 30, 2017).
- (28) Dunning, T. H., Jr. Gaussian Basis Sets for Use in Correlated Molecular Calculations. I. The Atoms Boron Through Neon and Hydrogen. *J. Chem. Phys.* **1989**, *90*, 1007–1023.
- (29) Czakó, G.; Szabó, I.; Telekes, H. On the Choice of the ab Initio Level of Theory for Potential Energy Surface Developments. *J. Phys. Chem. A* **2014**, *118*, 646–654.